iScience

CellPress
OPEN ACCESS

Article

# Direct-ink-write printing of hydrogels using dilute inks

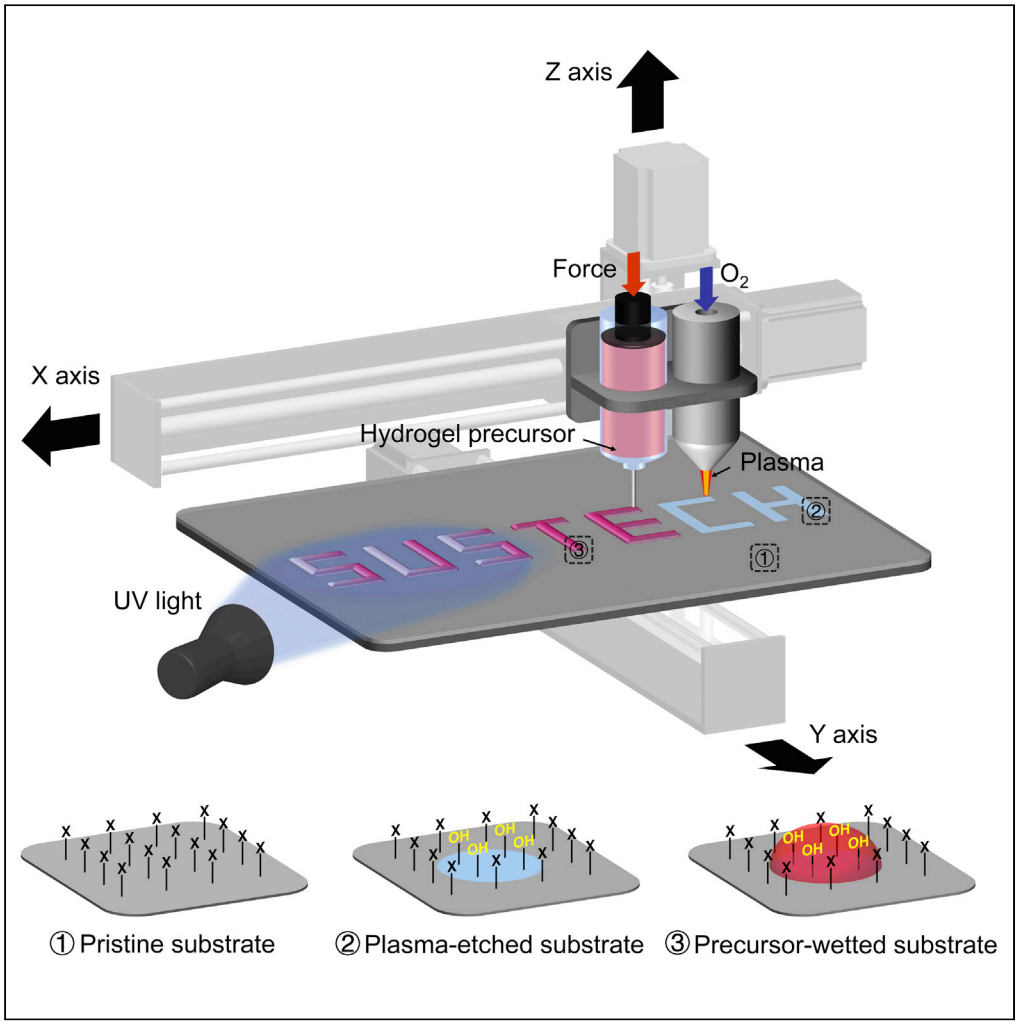


Xiaotian Li, Ping Zhang, Qi Li, Huiru Wang, Canhui Yang

yangch@sustech.edu.cn

## Highlights

Direct-ink-write printing is advanced to be compatible with dilute ink ($10^{-3}$ Pa·s)

The interaction between ink and substrate is mediated by tuning surface energies

The method is applicable for printing various materials on various substrates

Li et al., iScience *24*, 102319
April 23, 2021 
https://doi.org/10.1016/j.isci.2021.102319

iScience

CellPress
OPEN ACCESS

Article

# Direct-ink-write printing of hydrogels using dilute inks

Xiaotian Li,[1] Ping Zhang,[1] Qi Li,[1] Huiru Wang,[1] and Canhui Yang[1,2,*]

## SUMMARY

**Direct-ink-write (DIW) printing has been used in myriad applications. Existing DIW printing relies on inks of specific rheology to compromise with printing process, imposing restrictions on the choice of printable materials. Reported ink viscosity ranges from $10^{-1}$ to $10^{3}$ Pa·s. Here we report a method to enable DIW printing that is compatible with dilute ink ($10^{-3}$ Pa·s) by manipulating the interactions between ink and substrate. By exemplifying hydrogel printing, we build a printing system and show that dilute ink of appropriate surface energy, once extruded, can spontaneously wet and reside within the region of higher surface energy on a substrate of lower surface energy, while resisting gravity and maintaining shape before solidification. We demonstrate the diversity for printing various materials on various substrates and three deployments immediately enabled by the proposed method. The method expands the range of printable materials for DIW printing and the toolbox for additive manufacturing.**

## INTRODUCTION

Past decades have witnessed the start of a new era featured with the revolutionary transformations in conventional industrial manufacturing and worldwide supply chains imposed by the advances in additive manufacturing (Lipson and Kurman, 2013; Truby and Lewis, 2016). Examples include the rapid production of accessories in aircraft and car, customized hearing-aid shells, orthopedics, orthotics, prosthesis, and dishes. Additive manufacturing has also been playing an increasingly important role in scientific researches by enabling the fabrication of architected materials and structures, such as artificial vascular systems (Grigoryan et al., 2019), functional tissue models (Ma et al., 2018), metamaterials (Chanda et al., 2011), and robotics (Bartlett et al., 2015; Cheng et al., 2019b), which possess previously inaccessible properties, facilitating numerous cutting-edge applications in biomedicine and engineering (Athukorala et al., 2021; Lin et al., 2019; Zhang et al., 2019a, 2021b). Among the many printing techniques of additive manufacturing, digital projection lithography (DLP), stereolithography (SLA), and direct-ink-write (DIW) printing are commonly used for printing soft materials (Wallin et al., 2018). Both DLP and SLA enable high-speed processing with high resolution on the order of 10 μm, but they are limited to photopolymerizable inks and could encounter unwanted mixing between materials (Ge et al., 2021). In comparison, DIW offers higher degree of flexibility in choosing inks, lower cost, and lower entry for integrating dissimilar materials, whereas the resolution of DIW is usually lower (Zhou et al., 2020).

In the DIW printing, a computer-controlled translation stage moves a pattern-generating device, typically an ink-deposition nozzle, to make materials with programmed components and architectures. Such operation mode normally applies to the print of soft materials, with demonstrated deployments as diverse as human tissues (Lee et al., 2019), microfluidics (Su et al., 2020), optical and electrical devices (Zhang et al., 2019b), functional composites (Smay et al., 2002), soft sensors (Muth et al., 2014), and soft robots (Wehner et al., 2016). Crucial to the feasibility of the ink has been the shear thinning property, that is, the ink flows through the deposition nozzle like a liquid when stressed above its yield strength and sets rapidly after deposition to expedite shape retention. As shear thinning is not inherent for most inks, many inks, especially the dilute ones, are excluded or otherwise indispensably require careful controls of the ink compositions and thus the rheological behaviors. However, depending on the material systems, the acquisition of printability may scratch other material properties such as optical transparency, mechanical resilience, and biomedical compatibility, while exerting additional technical efforts to optimize the printing parameters such as the rate of ink extrusion, the moving speed of nozzle, and the magnitude of pressure source. From this perspective, the specific demands on the

[1]Department of Mechanics and Aerospace Engineering, Southern University of Science and Technology, Shenzhen 518055, China

[2]Lead contact

*Correspondence: yangch@sustech.edu.cn

https://doi.org/10.1016/j.isci.2021.102319

shear thinning of ink, although beneficial for printing on one hand, indeed hamper the applicability of DIW printing on the other hand.

DIW printing of hydrogels is such a representative example. As a large amount of water infiltrated polymer networks, hydrogels are featured as soft, transparent, biocompatible, stretchable, and conductive and have been pervasively used in daily life and in research frontiers with enumerations ranging from contact lenses (Wichterle and Lím, 1960), cosmetics, and diapers (Dubrovskii et al., 1990) to cell culture (Thiele et al., 2014), tissue engineering (Lee and Mooney, 2001), drug delivery (Li and Mooney, 2016), and more recently devices (Yang and Suo, 2018), robots (Lee et al., 2020), and machines (Liu et al., 2020). Advances in DIW printing, together with other advanced manufacturing techniques, are promoting further developments for hydrogels, by endowing hydrogels with programmed highly ordered, interconnected, and/or porous, as well as user-specified structures. Many fascinating applications of hydrogels are exploited in creating stretchable and transparent ionic circuits (Tian et al., 2017), living responsive devices (Liu et al., 2018b), *in vitro* reconstruction of organs (Grigoryan et al., 2019), and integrated structures of dissimilar materials (Yang et al., 2019). Unfortunately, for most hydrogels synthesized from the polymerization and cross-linking of monomers, the precursor is normally water-like dilute due to the high water content, up to 90% by weight or even higher. It is difficult to use a dilute hydrogel precursor, which generally encompasses the optimized constituents, as the ink for DIW printing. The viscosity of the ink has to be increased to compromise with the printing process, by adding rheological modifiers such as nanoclays (Hong et al., 2015) and long-chain polymers (Bakarich et al., 2013) or by pre-cross-linking (Ouyang et al., 2017). However, the increase of viscosity is often detrimentally associated with the modification of the printing system or the constituents of hydrogel precursor. For example, the tough alginate-polyacrylamide hydrogel curtails its ultimate elongation dramatically from more than 1,000% (Sun et al., 2012; Yang et al., 2013) down to about 300% (Bakarich et al., 2013) for the gain of printability. These discussions imply that existing concerns about the ink for DIW printing are mostly focused on the cohesive properties of the ink, whereas the role of the substrate is overlooked. A recent attempt uses the capacitor edge effect based on asymmetric capacitors to trap and pattern liquid and thus circumvent the modification of ink, but the pre-requisite built-in electrodes restrict the designing flexibility (Wang et al., 2019).

Here, by using the printing of hydrogel as the specific embodiment, we describe an approach to realize DIW printing using dilute inks, by manipulating the interactions between the ink and the substrate. Provided a substrate containing regions of different surface energies, the dilute ink of appropriate surface energy, once extruded, can spontaneously wet and reside within the regions of higher surface energy, while resisting gravitational fluid flow and maintaining shape. To take such advantages, we customize and assemble a printing system, equip it with a plasma torch, use *in situ* plasma etching to engender regions of different surface energies on a substrate, print, and photolytically cure a hydrogel precursor in 1 minute using UV illumination. We formulate an inviscid hydrogel precursor of optimized constituents and viscosity of ~0.008 Pa·s and use the as-prepared precursor as the ink for DIW printing. We carry out experiments to investigate the influences of relevant parameters of the plasma etching on printing qualities and the adhesion between printed hydrogel and substrate. We also show that the printing principle is generic and applies to various hydrogels on various substrates. We demonstrate the potential applications for printed ionic circuits, ionotronic luminescent devices, and soft large-strain sensors for soft pneumatic muscles. We envision that the proposed method broadens the choices of printable materials for DIW printing and expands the design space for additive manufacturing.

## RESULTS AND DISCUSSION

### Apparatus and principle of printing

The apparatus and principle of printing are schematized in Figure 1. The printing apparatus consists of a precision positioning system, an ink extruding system, and a controlling system, as well as a plasma torch for plasma generation. The controlling system controls the moving speed of the deposition nozzle, the position of XYZ direction, and the rate of ink extrusion relative to the sample stage. The exploded view of key modules of the home-made printing system is illustrated in Figure 1B. The pedestal is designed and manufactured by 3D printing using polylactic acid and used to fasten the plasma torch and the ink extrusion system, namely, the syringe. A parallel structure nozzle module with fixed gap is employed such that only one route needs to be programmed. The linear module is used to produce propulsive force for extruding ink. The plasma torch is used for plasma generation. The syringe is the reservoir for ink, and the fixture is to keep the syringe in place. Figure 1C shows the digital image of the printing system. We

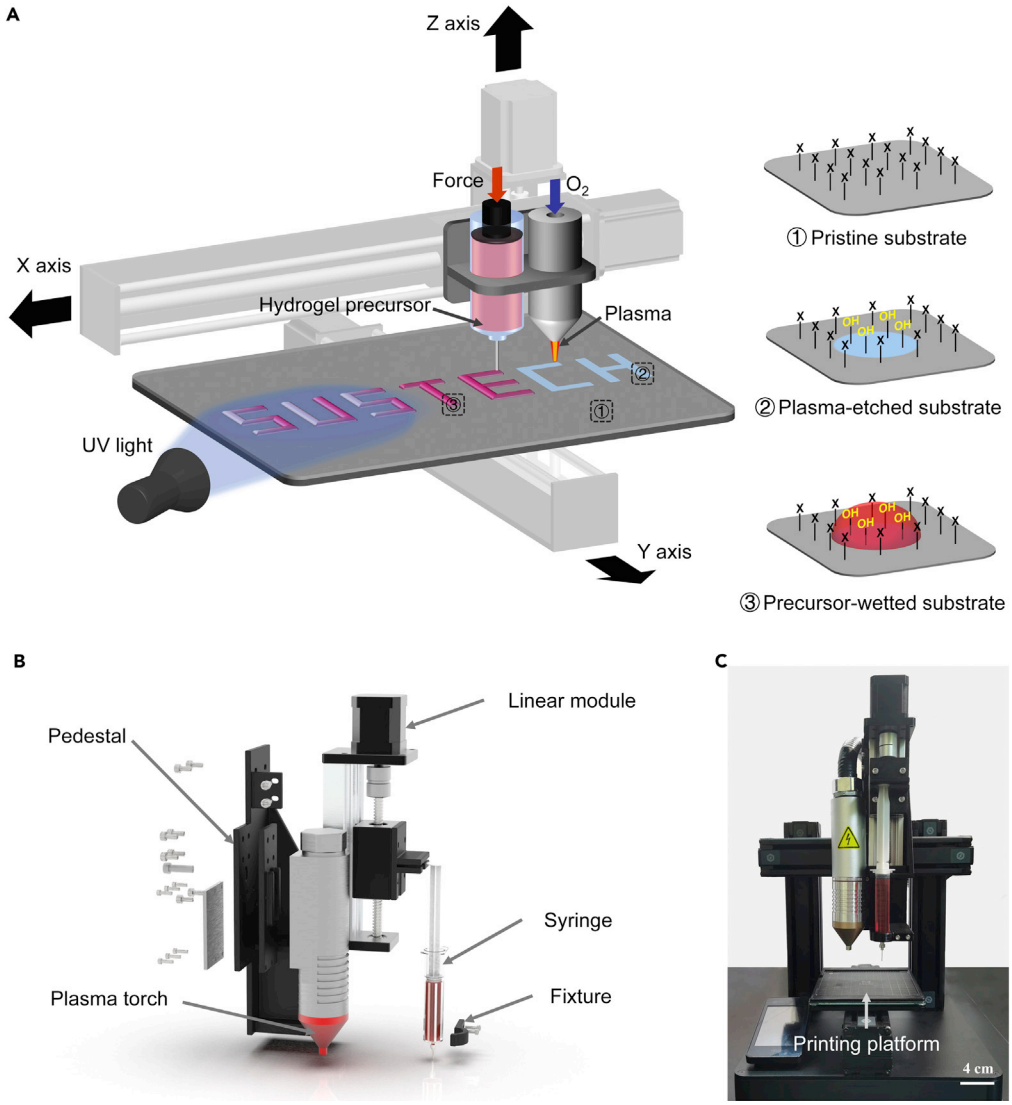


**Figure 1. Printing apparatus and printing principle**

(A) The printing apparatus consists of a precision positioning system, a plasma torch, an ink extruding system, and a controlling system (no shown). Before printing, the pristine substrate is uniformly covered by moieties *X*. Upon printing, oxygen is fed through the plasma torch, generating oxygen plasma to bombard the substrate. The bombarded regions (in blue) encompass higher surface energy than the other and are imparted with hydrophilic moieties (e.g., -OH groups). Subsequently, a force is applied on the ink extruding system to squeeze out the hydrogel precursor. The precursor (in red), of optimized recipe and without any deliberate rheological modifier, spontaneously wets and resides within the regions of higher surface energy. Finally, UV light is illuminated to solidify the precursor.

(B) Exploded view of printing module, including a linear module, a pedestal, a plasma torch, a syringe, and a fixture. (C) Digital image of the home-made printing system.

employ the atmospheric pressure plasma etching technology such that the plasma torch produces a strong interior electromagnetic field to ionize oxygen gas. Before printing, the pristine substrate is uniform and covered by moieties *X*. Upon printing, oxygen gas is fed through the plasma torch and ionized, and then it blows as a visible luminous electric arc at the outlet of the plasma torch. The bombardment of oxygen plasma increases the surface energy of etched region (in blue), by subtracting moieties *X* and engrafting hydrophilic moieties such as hydroxyl groups. After the plasma torch marches along a programmed route, the once uniform substrate contains regions of different surface energies. Subsequently, a force is applied on the ink extruding system to squeeze the hydrogel precursor out of the deposition nozzle. As the deposition nozzle marches along the same programmed route, the precursor (in red), of optimized

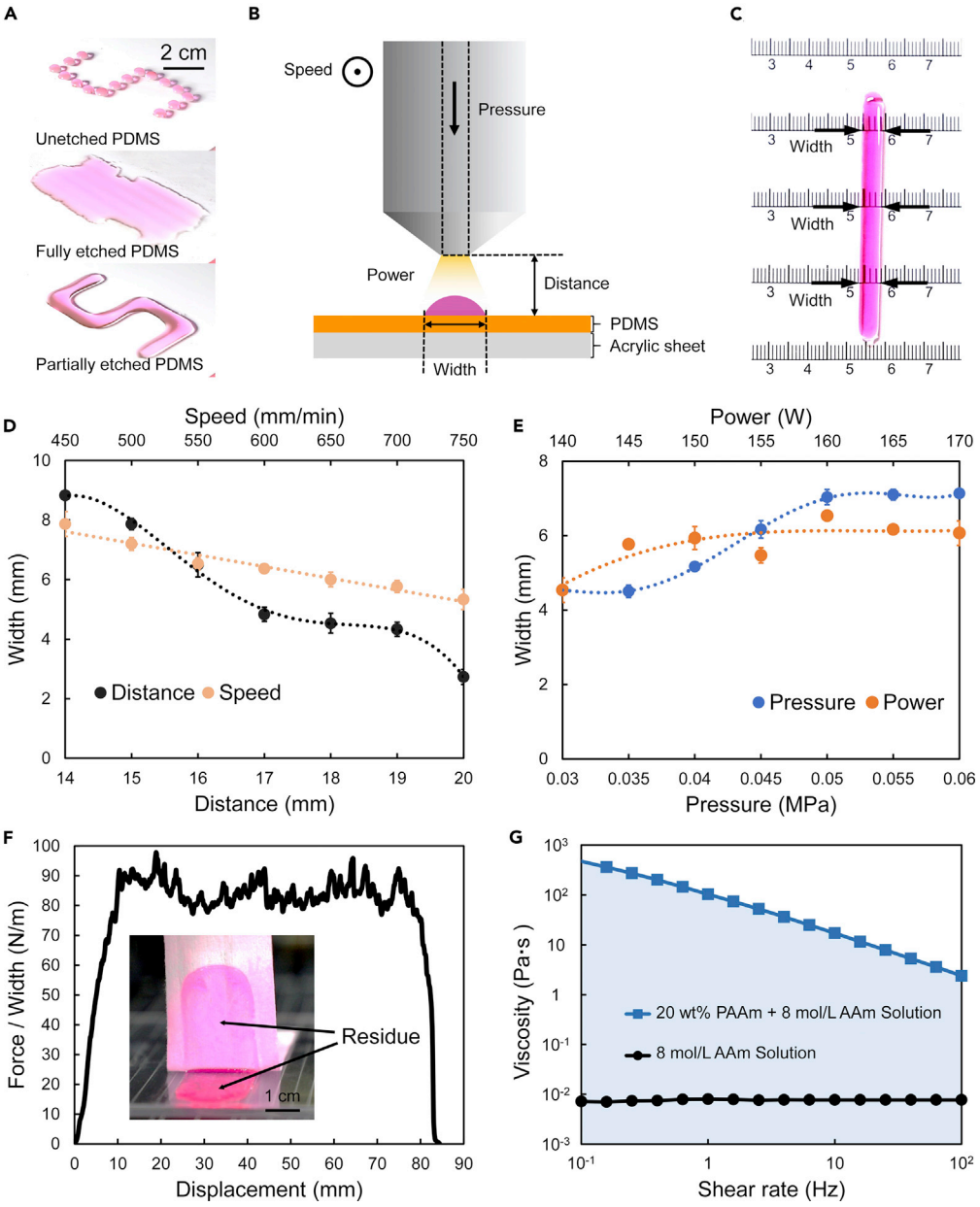


**Figure 2. Characterizations of printing**

(A) Digital images showing distinct wetting behaviors of PAAm hydrogel precursor on different substrates: beading up on unetched PDMS elastomer (top), spreading out on fully etched PDMS elastomer (middle), and designated wetting on partially etched PDMS elastomer (bottom).

(B) Schematic showing the pertinent parameters, including moving speed and power of plasma torch, pressure of oxygen, and the distance between the tip of plasma torch and the surface of PDMS elastomer.

(C) Illustration of the measurement of the width of a hydrogel line.

(D) Width of hydrogel line varies with distance and speed. For varying distance, the pressure is 0.03 MPa, speed 650 mm/min, and power 140 W. For varying speed, the pressure is 0.03 MPa, power 140 W, and distance 16 mm.

(E) Width of hydrogel line varies with pressure and power. For varying pressure, the speed is 650 mm/min, power 140 W, and distance 18 mm. For varying power, the pressure is 0.03 MPa, speed 650 mm/min, and distance 18 mm.

(F) Force/width-displacement curve of 90-degree peel of PAAm hydrogel from PDMS elastomer. Only one representative curve is shown for clarity. The inset illustrates a snapshot during peel, indicating cohesive failure.

(G) Viscosity-shear rate curves for the most dilute precursor containing 8 mol $L^{-1}$ AAm (black) and the most viscous precursor containing 20 wt % PAAm and 8 mol $L^{-1}$ AAm (blue) used in our experiments for an extrusion rate of

**Figure 2. *Continued***
$q_v$ = 1.714 mL min$^{-1}$. In principle, any ink with viscosity located in the blue-shaded zone is printable without any modification of the printing machine. The viscosity of printable material varies across about 5 orders of magnitude at a shear rate of 1 Hz.

recipe and without any deliberate rheological modifier, will wet and stay within the regions of higher surface energy spontaneously. Finally, UV light is illuminated to cure the precursor into a hydrogel.

## Characterizations of printing

Although the proposed principle of printing can be illustrated using various material systems, we select the commonly used polyacrylamide (PAAm) hydrogel synthesized by the free radical polymerization of monomers and polydimethylsiloxane (PDMS, Sylgard 184 at a weight ratio of cross-linking agent to base of 1:10) elastomer. Abundant in methyl groups, the surface of PDMS elastomer is naturally hydrophobic with a surface energy ranging between 20 and 30 mJ m$^{-2}$. In contrast, the precursor of PAAm hydrogel contains plenty of water of surface energy ~70 mJ m$^{-2}$, resulting in the dewetting on PDMS elastomer (Figure S1A). The surface of PDMS elastomer can be converted into hydrophilic via surface treatment such as plasma etching. The treated surface exposes ample hydroxyl groups and allows the hydrogel precursor to almost thoroughly wet (Figure S1B). However, in both cases the hydrogel precursor cannot retain shape after deposition. One has to increase the viscosity for the sake of printability on a substrate of uniform surface energy. Nevertheless, when the substrate is partially plasma etched to have non-uniform surface energies, that is some regions have higher surface energy than that of the other, the hydrogel precursor can reside within the regions of higher surface energy (Figure S1C) (Zhang et al., 2021a). Remarkably, the shape of dilute ink after deposition can be continuously tuned by simply changing the volume and well maintaining on partially plasma-etched substrate (Figure S2). To delineate the prominent effects of surface energy on the wetting behaviors of dilute ink, we formulate a hydrogel precursor containing 8 mol L$^{-1}$ acrylamide (AAm) monomer, use it as the ink, and print the ink on PDMS elastomers having various surface energy morphologies. The printing route is programmed to display the letter "S" (see Note S1 for the G-code for patterning "S"). Distinctly different wetting behaviors are observed (Video S1) that the ink dewets and beads up on unetched PDMS elastomer (Figure 2A, top), spreads out on fully etched PDMS elastomer (Figure 2A, middle), and resides within plasma-etched regions on partially etched PDMS elastomer (Figure 2A, bottom). The partially etched PDMS elastomer possessing different surface energies allows for designated wetting and stable shape maintenance of the ink before solidification.

Now that we can program the pattern of the regions of higher surface energy on a substrate of lower surface energy, we continue to investigate the influences of pertinent parameters, including moving speed and power of plasma torch, pressure of oxygen, and the distance between the tip of plasma torch and the surface of PDMS elastomer, on the printing quality (Figure 2B). We print the ink into a straight line on a layer of PDMS elastomer, which is spin-coated on an acrylic sheet; cure the ink into a hydrogel; and measure the width of the hydrogel line. Because the acrylic sheet, PDMS elastomer, and hydrogel are all transparent, the width can be measured through the readings of the tick marks underneath the sample (Figure 2C). Three positions are selected at the top, middle, and bottom of the line and measured, and their average gives the width. Recall that the ink wets the regions of higher surface energy, so the width of plasma-etched region determines the width of the hydrogel line. As shown in Figure 2D, the width of the hydrogel line narrows when the moving speed becomes faster or the distance increases, which should be due to the rapid neutralization of the charged species in air. Oppositely, the increment of either the power of plasma torch or the pressure of oxygen gas widens the width of hydrogel line at the beginning and then plateaus (Figure 2E). It should be pointed out here that, in addition to the width of hydrogel line, the effectiveness of plasma etching, i.e., the hydrophilicity of the surface of PDMS elastomer after plasma treatment, is also an important concern, because the hydrogel line will break without a sufficiently hydrophilic pattern. With this in mind, the scope of the four pertinent parameters is selected by considering the effectiveness of plasma etching and the capability of the equipment. A 3-mm-wide hydrogel line is obtained at a moving speed 650 mm min$^{-1}$, power of plasma torch 140 W, pressure of oxygen 0.03 MPa, and distance of 20 mm.

In our experiments, the curing of the ink proceeds in open air, whereas free radical polymerization is known to be prohibited by oxygen. Normally, the curing process needs to proceed in an oxygen-free environment, either in hermetic molds or in glove box infiltrated with gases such as nitrogen and argon. Here we mitigate

the adverse effects of oxygen by using a high monomer concentration of 8 mol $L^{-1}$ and the photo-initiator lithium phenyl-2,4,6-trimethylbenzoylphosphinate (LAP). LAP is water-soluble and can produce free radicals with high efficacy under UV irradiation. The synergy of high monomer concentration and LAP ensures that the rate of free radical generation surpasses the rate of free radical quenching by oxygen, so the free radical polymerization proceeds fast and sufficiently before the ambient oxygen dissolves and diffuses into the ink (Guvendiren et al., 2010). Compared with the hydrogel synthesized by conventional molding method, the hydrogel cured with LAP exhibits comparable mechanical properties (Figure S3). We print and cure a PAAm hydrogel "SUSTECH" pattern on a sheet of PDMS elastomer (Figure S4), with the entire operation completed in ambient condition (Figure S5). The adverse effects of oxygen might be circumvented by curing the hydrogel with oxygen tolerant processes such as self-assembly of macromolecules and ring-opening reactions.

The integration of hydrogels and hydrophobic elastomers has enabled many emerging and exciting applications (Keplinger et al., 2013; Yang et al., 2015). However, their dissimilar chemistries and the large amount of water in hydrogel lead to the lack of interfacial adhesion, which is "mission-critical" for most practical uses. In this regard, we add vinyl silanes (3-(trimethoxysilyl)-propyl methacrylate [TMSPMA]) into the ink and copolymerize them with the monomers. The amount of silanes (1.2 mol % with respect to AAm) is small so the addition of silanes barely interferes with the rheology of the ink. Because the plasma-etched regions contain vast hydroxyl groups, the silanes-engrafted polymer chains can covalently anchor onto the substrate via silane condensation (Liu et al., 2018a), resulting in strong adhesion between the printed hydrogel and elastomer. We print a sheet of PAAm hydrogel on the surface of PDMS elastomer, characterize the adhesion by 90-degree peel (Figure S6A), and record the force/width as a function of displacement (Figure 2F). Cohesive failure ensues, as shown by the inset in Figure 2F, and hydrogel residues are left on both the backing layer and the substrate (Figure S6B), indicating that the adhesion between the hydrogel and elastomer is greater than the toughness of hydrogel. The averaged plateau force/width gives an adhesion of 71.4 J $m^{-2}$.

In general, the viscosity of ink for the DIW printing of hydrogel needs to be significantly increased for shear thinning property. For instance, long-chain polymers are incorporated into the ink, raising the viscosity from the order of $10^{-3}$ Pa·s (water-dilute) to the order of $10^{3}$ Pa·s, for printing hydrogel ionic circuits (Tian et al., 2017). Rather, the proposed printing principle depends on the interactions between the ink and the substrate. Consequently, inks that are dilute and are not shear thinning can also be printed. We characterize the viscosity of the ink containing 8 mol $L^{-1}$ AAm as a function of shear rate, and a constant viscosity of ~0.008 Pa·s is obtained when the shear rate varies from $10^{-1}$ to $10^{2}$ Hz (Figure 2G). Of course, deionized water ($10^{-3}$ Pa·s) can also be printed. Moreover, the printing system retains printing capability without changing its mechanical structures when 20 wt % PAAm chains are added into the AAm solution to boost the viscosity to $10^{2}$ Pa·s, characterized at a shear rate of 1 Hz, at an extrusion rate of the ink $q_v$ = 1.714 mL $min^{-1}$. After deposition, we observe that the viscous ink does not wet through the plasma-etched region, which resembles the phenomena in conventional DIW printing and implies the predominance of the cohesive strength. In principle, any ink in the blue-shaded zone in Figure 2G can be printed. The viscosity of printable material varies across about 5 orders of magnitude at a shear rate of 1 Hz. The range of printable materials for DIW printing is expanded significantly.

## Diversity of printing

The proposed principle of printing relies on the selective wetting of ink of appropriate surface energy on the substrate containing regions of different surface energies. Unlike conventional DIW printing where the ink compositions or the mechanical components need to be redesigned whenever the printing material is changed, our method readily applies to the DIW printing of various materials on various substrates. Again, by exemplifying the printing of hydrogel, we print seven types of hydrogels, each representing a family of functional hydrogels, on PDMS elastomer. They are neutral (AAm), anionic (2-acrylamido-2-methylpropane sulfonic acid [AMPS]), cationic ([3-(methacryloylamino)propyl]trimethylammonium chloride, MAPTAC), zwitterionic ([2-(methacryloyloxy)ethyl]dimethyl-(3-sulfopropyl) ammonium hydroxide [SPE]), pH-responsive (acrylic acid [AAc]), temperature-responsive (N-isopropylacrylamide [NIPAM]), and natural polymer-based (gelatin-methacryloyl [GelMA]) hydrogels. The chemical structures of the monomers/polymers of the selected hydrogels are shown in Figure 3A. For each type of hydrogel, we formulate a dilute ink, print a sheet of hydrogel on a PDMS elastomer, and subject the bilayer sample to 90-degree peel. Because MAPTAC monomer solution by itself does not cure, we copolymerize MAPTAC with AAm to form a

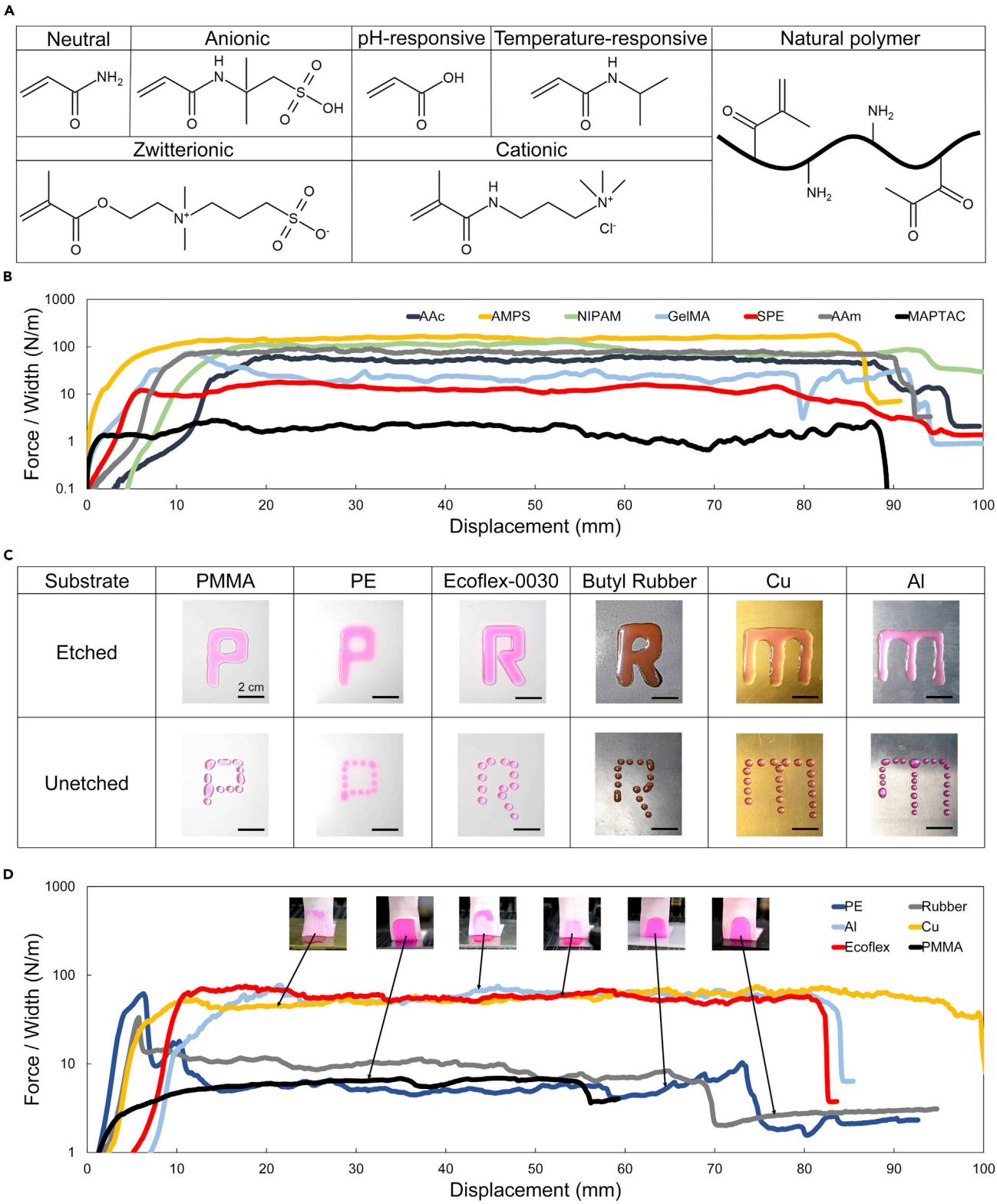


**Figure 3. Diversity of printable hydrogels and substrates**

(A) Chemical structures of the monomers/polymers of representative printable hydrogels, including AAm (neutral), 2-acrylamido-2-methylpropane sulfonic acid (AMPS, anionic), acrylic acid (AAc, pH-responsive), N-isopropylacrylamide (NIPAM, temperature-responsive), [2-(methacryloyloxy)ethyl]

**Figure 3. *Continued***

dimethyl-(3-sulfopropyl)ammonium Hydroxide (SPE, zwitterionic), [3-(methacryloylamino)propyl]trimethylammonium chloride (MAPTAC, cationic), and gelatin-methacryloyl (GelMA, natural polymer).

(B) Force/width-displacement curves of various printed hydrogels on PDMS elastomer by 90-degree peel. Only one representative curve for each type of hydrogel is shown for clarity.

(C) Printing PAAm hydrogels on various substrates, including poly(methyl methacrylate) (PMMA, plastic), polyester (PE, plastic), Ecoflex-0030 (silicon rubber), butyl rubber, copper (Cu, metal), and aluminum (Al, metal). Designated patterns are obtained with plasma etching (top row), whereas discrete beads are obtained without plasma etching (bottom row). The letter "P" represents "Plastic," "R" represents "Rubber," and "m" represents "Metal."

(D) Force/width-displacement curves of printed PAAm hydrogels on various substrates by 90-degree peel. Only one representative curve is shown for each type of substrate for clarity. The insets show snapshots during peel.

copolymer hydrogel. The force/width versus displacement curves are collected in Figure 3B, giving adhesion of 71.4 J $m^{-2}$ for PAAm, 151.6 J $m^{-2}$ for PAMPS, 1.7 J $m^{-2}$ for PMAPTAC, 10.5 J $m^{-2}$ for PSPE, 53.3 J $m^{-2}$ for PAAc, 94.9 J $m^{-2}$ for PNIPAM, and 26.9 J $m^{-2}$ for GelMA. It is noted that cohesive failure occurs for PAAm/PAMPS/PNIPAM/PSPE/PMAPTAC hydrogels, whereas adhesive failure occurs for PAAc and GelMA hydrogels (Video S2). The low pH value of the ink of PAAc hydrogel is the plausible reason for the weak adhesion, provided the rapid condensation between silanes at low pH (Liu et al., 2018a). As for GelMA, our rudimentary recipe yields a stiff yet fragile hydrogel and the low adhesion should be ascribed to the high bulk stiffness.

We further demonstrate the diversity of the proposed printing principle by varying the substrates. We select three classes of materials, plastic, rubber, and metal, with each exemplified by two specific examples. As tabulated in Figure 3C, we print PAAm hydrogel on pristine/plasma-etched poly(methyl methacrylate) (PMMA, plastic), polyester (PE, plastic), Ecoflex-0030 (silicon rubber), butyl rubber, copper (Cu, metal), and aluminum (Al, metal). The colored dilute inks consistently wet the plasma-etched regions to form designated patterns, whereas they form discrete liquid beads on pristine substrate (Video S3). We note that, regardless of different surface energies of different pristine substrates used here, plasma etching can generate regions of higher surface energy such that designated wetting becomes feasible. Nevertheless, designated wetting fails when the surface energy of the substrate, e.g., glass, undergoes only slight increase after plasma etching. To what extent the difference of surface energy is adequate should strongly depend on the material systems and the surface treatment method and will be discussed later. We also characterize the adhesion between printed PAAm hydrogel and various substrates by 90-degree peel (Figure 3D). Cohesive failure occurs for the PAAm on Cu, Al, and Ecoflex-0030, giving adhesion of 55.7 J $m^{-2}$, 59.6 J $m^{-2}$, and 59.4 J $m^{-2}$, respectively. These values are comparable to that on PDMS elastomer, which is merited because crack propagates through hydrogel instead of interface (Video S4) so that adhesion is determined by the toughness of PAAm hydrogel. Adhesive failure occurs for the other three substrates, with adhesion of 6.2 J $m^{-2}$, 5.9 J $m^{-2}$, and 9.7 J $m^{-2}$ for PMMA, PE and butyl rubber, respectively. The understanding is as follows. After plasma etching, the surfaces of metal and silicon rubber get rich in hydroxyl groups and form covalent interlinks with PAAm hydrogel through silane condensation. However, the surface of polymeric substrates with the backbones made of carbon chains (i.e., PMMA, PE, and butyl rubber), although possessing higher surface energy and becoming hydrophilic after plasma etching, can only adhere to PAAm hydrogel through physical interactions.

## Printed circuits, ionotronics, and sensors for soft robots

As noted in the beginning, advanced manufacturing techniques are enabling fascinating applications for hydrogels. Here we elucidate three potential applications immediately enabled by the DIW printing based on the proposed printing principle. Unless otherwise specified, the ink is made of 8 mol $L^{-1}$ AAm solution containing 10 mol $L^{-1}$ lithium chloride (LiCl). First, we print ionic circuits with controlled electrical properties. We program and plasma-etch three rectangular regions of identical length and width on a PDMS elastomer and eject and cure different volumes of ink (Figure 4A). Regard the hydrogel as an incompressible ideal resistor and recall that the resistance is correlated to geometry as $R = \rho L/A = \rho L^2/V$, where $R$ is resistance of unit $\Omega$, $\rho$ is resistivity of unit $\Omega$ m, $L$ is length of unit m, $A$ is cross-sectional area of unit $m^2$, and $V$ is volume of unit $m^3$. Because the three hydrogel lines have the same length, their cross-sectional area is proportional to the volume. Consequently, the resistance is inversely proportional to the volume. For the width of 9 mm, the experimentally measured resistance, using the four-point method, diminishes with increasing volume as expected (Figure 4B). When the length of the three rectangular regions and the volume of ink are equal, the cross-sectional area will be equal as well, whereas the shape of cross-section varies with the width (Figure 4C). In this case, the three hydrogel lines will have the same resistance, as manifested by

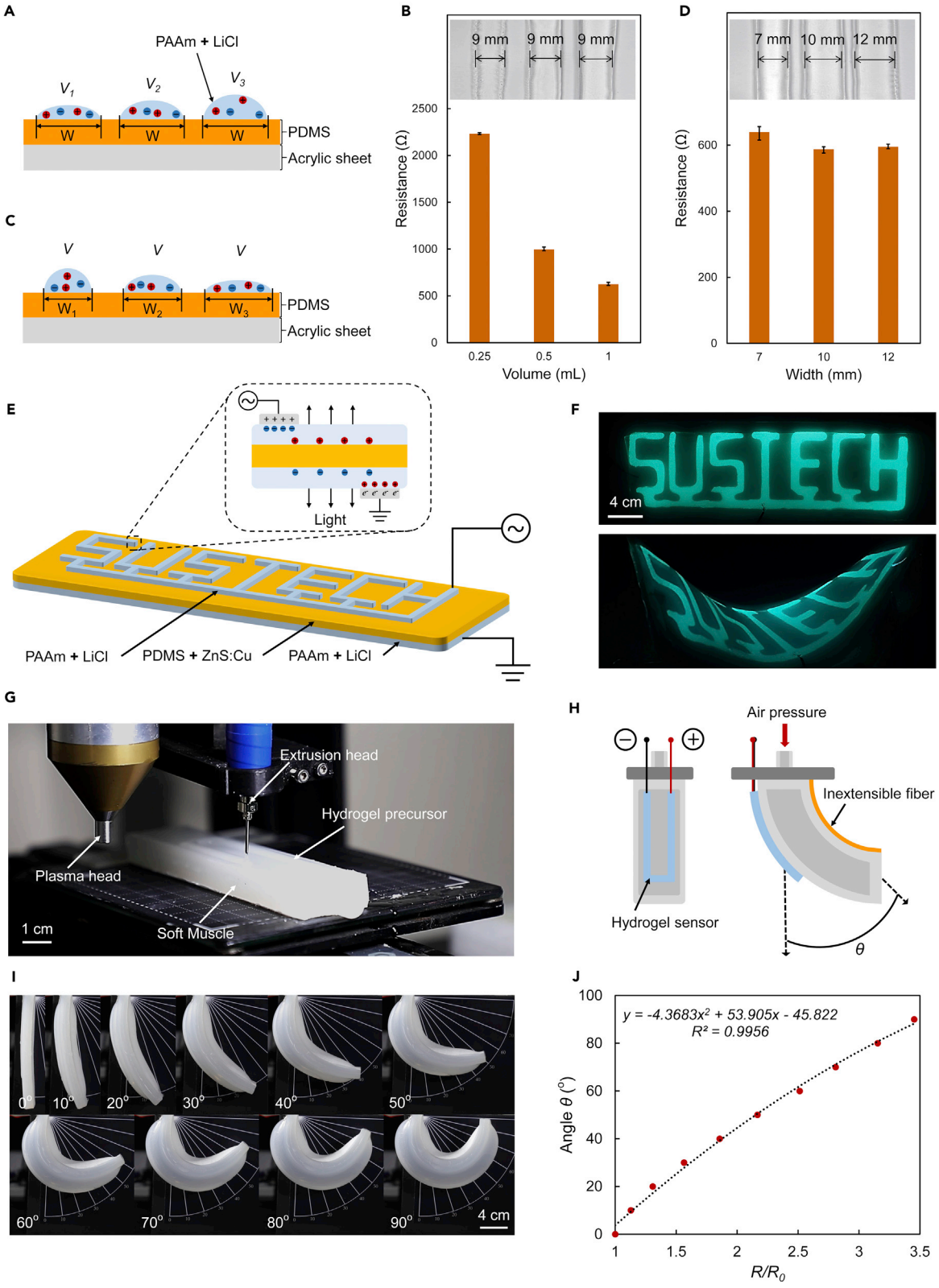
A
PAAm + LiCl
V1
V2
V3
W
W
W
PDMS
Acrylic sheet
B
9 mm
9 mm
9 mm
Resistance (Ω)
2500
2000
1500
1000
500
0
0.25
0.5
1
Volume (mL)
D
7 mm
10 mm
12 mm
Resistance (Ω)
600
400
200
0
7
10
12
Width (mm)
C
V
V
V
W1
W2
W3
PDMS
Acrylic sheet
E
Light
PAAm + LiCl
PDMS + ZnS:Cu
PAAm + LiCl
F
4 cm
G
Extrusion head
Hydrogel precursor
Plasma head
1 cm
Soft Muscle
H
Air pressure
Inextensible fiber
Hydrogel sensor
θ
I
0°
10°
20°
30°
40°
50°
60°
70°
80°
90°
4 cm
J
y = -4.3683x² + 53.905x - 45.822
R² = 0.9956
Angle θ (°)
100
80
60
40
20
0
1
1.5
2
2.5
3
3.5
R/R0

**Figure 4. Printed ionic circuits, hydrogel ionotronics, and stretchable sensors for soft robots**

(A) The cross-sectional area of printed hydrogel line increases proportionally with volume, provided constant width and length.

(B) Resistances of hydrogel lines with the same width and length but different volumes. Insets: samples of width 9 mm and volume 0.25/0.5/1 mL, respectively.

(C) Regardless of the width, the cross-sectional area of the printed hydrogel line is constant, provided constant length and volume.

(D) Resistances of hydrogel lines with the same length and volume but different widths. Insets: samples of volume 1 mL and different widths as indicated.

(E) Architecture and working principle of a hydrogel ionotronic luminescent device.

(F) A luminescent "SUSTECH" logo is fabricated by patterning hydrogels on luminescent layer. The luminescent device is soft and stretchable such that it can be crimped or twisted while maintaining luminescence.

(G) A snapshot during the *in situ* printing of a hydrogel sensor on a soft muscle made of silicon rubber Ecoflex-0050.

(H) Schematic illustrating the measure of the deformation of the soft muscle through the measure of the resistance of the hydrogel sensor. Bending angle is defined as indicated.

(I) A sequence of images showing the deformation process of the soft muscle without delamination of the hydrogel sensor, which is on the left side.

(J) Bending angle versus relative resistance change.

experiments (Figure 4D). The programmable electrical properties of hydrogels by simply programming the printing parameters are beneficial for rapid prototyping of soft stretchable and transparent ionic circuits of various kinds.

We then print hydrogel electrodes of programmed pattern to achieve ionotronic luminescence (Larson et al., 2016; Yang et al, 2016, 2020). The schematic and working principle of the lamellar device are illustrated in Figure 4E. The device consists of a luminescent layer, made of copper-doped zinc sulfide (ZnS:Cu) phosphor particles-dispersed PDMS elastomer and two layers of PAAm hydrogels containing lithium chloride. The two hydrogels connect to an external power source and grounds, respectively, through copper wires. When the external power source applies an alternating voltage, ions of opposite polarities periodically accumulate at the top and bottom surfaces of the luminescent layer, producing electric field to trigger the phosphor particles to emit light. Electrons in copper and ions in PAAm hydrogel meet at the interface and form electric double layers, which behave like capacitors so long as the voltage drop is within the electrochemical window. In a fabricated device, the bottom hydrogel is a large sheet, whereas the top hydrogel is patterned. Only the phosphor particles located in between the two hydrogel layers emit light when voltage is applied. We print the hydrogel electrodes into "SUSTECH" pattern and apply voltage to trigger luminescence (Figure 4F). As both PAAm hydrogel and PDMS elastomer are soft and stretchable, the device is also soft and stretchable that it can be crimped or twisted while maintaining luminescence.

We further print hydrogels as the soft stretchable sensors for soft robots. Whereas soft robots surpass their rigid counterparts in many ways, to preserve their adaptivity and safety, they require sensors that are soft, stretchable, and conformable, which are essentially the merits of hydrogels. As a specific deployment, we fabricate a soft muscle, that is a pneumatic chamber, using the silicon elastomer Ecoflex-0050 (Figure S7). As the deformation of the soft muscle cannot be solely determined by pressure, a sensor that can cooperate with the soft muscle is needed. It has been demonstrated that hydrogels can serve the functions (Cheng et al., 2019a), but preceding work relies on manual assembly, which is awkward in terms of manufacturing speed, accuracy, and consistency, compared with 3D printing. Here we directly print and cure the hydrogel sensor on the soft muscle (Figure 4G). Strong adhesion is achieved in the assistance of silanes. We characterize the sensor-muscle system as follows (Figure 4H). The soft muscle is connected to an air pressure source, constrained by a soft but inextensible layer on one side and adhered to the hydrogel sensor on the other side. The hydrogel sensor is connected to an external circuit and in series with an amperemeter. As the air pressure source inflates the soft muscle, the hydrogel sensor deforms accordingly, resulting in the change of resistance and thus the current of the amperemeter. During actuation, the current of amperemeter varies synchronously with the pressure (Video S5). The angle made by the vertical line and the line between the central points of two terminals of soft muscle defines the bending angle. The operation of the system is recorded using a digital camera (Canon, EOS 6D Mark II), and the video is post-processed for analysis. A sequence of snapshots shows the deformation process of the soft muscle without delamination of the hydrogel sensor (Figure 4I). The relation between the bending angle and relative resistance change is plotted in Figure 4J and can be well approximated by a simple quadratic polynomial function. In practice, a calibration step determines the fitting function then the configuration of the soft muscle can be monitored electrically.

We have argued that our principle is valid for dilute inks of appropriate surface energy. However, what surface energy is appropriate? We note the following two basic requirements: (1) the surface energy of

plasma-etched region, $\gamma_2$, should be larger than that of pristine substrate, $\gamma_1$ and (2) the surface energy of the ink, $\gamma_3$, should also be larger than $\gamma_1$, and preferably be smaller than $\gamma_2$ at the same time. The first requirement $\gamma_2 > \gamma_1$ is satisfied in our experiments except for glass where the surface energy changes negligibly after plasma etching. As for the second requirement, if $\gamma_3 < \gamma_1$, then it will be energetically favorable for the ink to spread over the pristine substrate. For example, when we use a perfluoropolyether oil (Krytox) of low surface energy (19 mJ $m^{-2}$) as the ink, the ink keeps spreading after deposition (Video S6). The almost thorough wetting of deionized water on fully plasma-etched PDMS elastomer implies their similar surface energy. If $\gamma_3 > \gamma_2$, then the ink will dewet and bead up, resembling a droplet of deionized water on PDMS elastomer. We further add surfactant sodium dodecyl sulfate (3 wt %) into deionized water such that the surface energy of the ink is lower than that of plasma-etched region but larger than that of pristine region on PDMS elastomer, i.e., $\gamma_1 < \gamma_3 < \gamma_2$, evidenced by the change of contact angle from obtuse to acute (Figure S8). As expected, printability is retained under such circumstance (Video S7). Definitely, the applicability of our printing system is not limited to hydrogel ink. Dilute inks that encompass suitable surface energy are all printable. To throw a sprat, we print and cure an "S"-shaped PAAm ionogel on PDMS elastomer using the ionic liquid 1-ethyl-3-methylimidazolium ethylsulfate ([C2mim][EtSO4]) (Figure S9 and Video S8). Furthermore, 3D printing on non-planar surface is feasible so long as surface tension prevails to stabilize designated wetting (Figure S10 and Video S9).

## Limitations of the study

Compared with existing DIW printing techniques, the technique developed in this work has the following advantages. First, it is compatible with a variety of hydrogels without adjusting their rheological properties, which is often time-consuming and detrimental for other material properties. Second, it is also compatible with a variety of substrates. Third, the ink extrusion rate is generally faster than the methods using viscous inks. For the same amount of ink extrusion, the execution time is on the order of magnitude 10 s in our experiments but is on the order of $10^3$ s otherwise. Despite the advantages, we note the need of further optimizations for our printing system. For example, the printing resolution is limited on the order of 1 mm, which is mainly bottlenecked by the resolution of plasma etching. Advanced technique such as soft lithography can be used to engender more elaborate patterns with higher surface energy than the surrounding. Currently, only one type of ink can be printed at a time. With multi-material printing technique (Skylar-Scott et al., 2019), the integrated printing of soft robot and soft sensor could be realized, which will greatly improve the integration and accuracy of manufacturing to promote one more step toward the control of soft robots. Moreover, whereas only potential applications of hydrogels as ionic conductors have been demonstrated, the functionalities of hydrogel are far beyond that. For example, the integrations of pH-responsive and temperature-responsive hydrogels with passive hydrogels/elastomers can function as drug vehicles, soft actuators, and robots (Liu et al., 2020). As another example, hydrogel-coated substrates unify the superior properties of the hydrogel (e.g., lubricity, biocompatibility, and drug release) and the superior properties of the substrate (e.g., stiffness, strength, and toughness), readily enabling broad applications in biomedicine and engineering (Liu et al., 2021).

In conclusion, we have described a method to enable DIW printing using dilute inks by manipulating the interactions between the ink and the substrate. We set up a printing system capable of in-site plasma etching and demonstrate the method by the printing of hydrogel. DIW printing using inks of viscosity on the order of $10^{-3}$ Pa·s is achieved, and the viscosity of printable inks varies across 5 orders of magnitude without modifying the printing machine. We have demonstrated the generality of the method by printing various materials on various substrates as well as three potential deployments. It is hoped that the proposed strategy will help broaden the design space for DIW printing and expand the toolbox for additive manufacturing.

## Resource availability

### *Lead contact*

Further information and requests for resources should be directed to and will be fulfilled by the lead contact, Canhui Yang (yangch@sustech.edu.cn).

### *Materials availability*

This study did not generate new unique reagents.

*Data and code availability*

The G-code for patterning "S" is described in Note S1.

## METHODS

All methods can be found in the accompanying transparent methods supplemental file.

## SUPPLEMENTAL INFORMATION

Supplemental information can be found online at https://doi.org/10.1016/j.isci.2021.102319.

## ACKNOWLEDGMENTS

The work at Southern University of Science and Technology is supported by Shenzhen Science and Technology Innovation Commission (JCYJ20190809181207442) and Guangdong Basic and Applied Basic Research Foundation (K20323004).

## AUTHOR CONTRIBUTIONS

X.L. and C.Y. conceived the idea. X.L. conducted experiments with some help of P.Z., Q.L, and H.W., analyzed data and prepared figures. X.L. and C.Y. wrote the manuscript. All authors discussed the results and commented on the manuscript.

## DECLARATION OF INTERESTS

The authors declare no completing interests.

Received: January 28, 2021
Revised: March 6, 2021
Accepted: March 14, 2021
Published: April 23, 2021

## REFERENCES

Athukorala, S.S., Tran, T.S., Balu, R., Truong, V.K., Chapman, J., Dutta, N.K., and Roy Choudhury, N. (2021). 3D printable electrically conductive hydrogel scaffolds for biomedical applications: a review. Polymers (Basel) *13*, 474.

Bakarich, S.E., Panhuis, M.I.H., Beirne, S., Wallace, G.G., and Spinks, G.M. (2013). Extrusion printing of ionic–covalent entanglement hydrogels with high toughness. J. Mater. Chem. B *1*, 4939–4946.

Bartlett, N.W., Tolley, M.T., Overvelde, J.T.B., Weaver, J.C., Mosadegh, B., Bertoldi, K., Whitesides, G.M., and Wood, R.J. (2015). A 3D-printed, functionally graded soft robot powered by combustion. Science *349*, 161–165.

Chanda, D., Shigeta, K., Gupta, S., Cain, T., Carlson, A., Mihi, A., Baca, A.J., Bogart, G.R., Braun, P., and Rogers, J.A. (2011). Large-area flexible 3D optical negative index metamaterial formed by nanotransfer printing. Nat. Nanotechnol. *6*, 402–407.

Cheng, S., Narang, Y.S., Yang, C., Suo, Z., and Howe, R.D. (2019a). Stick-on large-strain sensors for soft robots. Adv. Mater. Interfaces *6*, 1900985.

Cheng, Y., Chan, K.H., Wang, X.-Q., Ding, T., Li, T., Lu, X., and Ho, G.W. (2019b). Direct-ink-write 3D printing of hydrogels into biomimetic soft robots. ACS Nano *13*, 13176–13184.

Dubrovskii, S.A., Afanas'eva, M.V., Lagutina, M.A., and Kazanskii, K.S. (1990). Comprehensive characterization of superabsorbent polymer hydrogels. Polym. Bull. *24*, 107–113.

Ge, Q., Chen, Z., Cheng, J., Zhang, B., Zhang, Y.-F., Li, H., He, X., Yuan, C., Liu, J., Magdassi, S., and Qu, S. (2021). 3D printing of highly stretchable hydrogel with diverse UV curable polymers. Sci. Adv. *7*, eaba4261.

Grigoryan, B., Paulsen, S.J., Corbett, D.C., Sazer, D.W., Fortin, C.L., Zaita, A.J., Greenfield, P.T., Calafat, N.J., Gounley, J.P., Ta, A.H., et al. (2019). Multivascular networks and functional intravascular topologies within biocompatible hydrogels. Science *364*, 458–464.

Guvendiren, M., Burdick, J.A., and Yang, S. (2010). Kinetic study of swelling-induced surface pattern formation and ordering in hydrogel films with depth-wise crosslinking gradient. Soft Matter *6*, 2044–2049.

Hong, S., Sycks, D., Chan, H.F., Lin, S., Lopez, G.P., Guilak, F., Leong, K.W., and Zhao, X. (2015). 3D printing of highly stretchable and tough hydrogels into complex, cellularized structures. Adv. Mater. *27*, 4035–4040.

Keplinger, C., Sun, J.-Y., Foo, C.C., Rothemund, P., Whitesides, G.M., and Suo, Z. (2013). Stretchable, transparent, ionic conductors. Science *341*, 984–987.

Larson, C., Peele, B., Li, S., Robinson, S., Totaro, M., Beccai, L., Mazzolai, B., and Shepherd, R. (2016). Highly stretchable electroluminescent skin for optical signaling and tactile sensing. Science *351*, 1071–1074.

Lee, A., Hudson, A.R., Shiwarski, D.J., Tashman, J.W., Hinton, T.J., Yerneni, S., Bliley, J.M., Campbell, P.G., and Feinberg, A.W. (2019). 3D bioprinting of collagen to rebuild components of the human heart. Science *365*, 482–487.

Lee, K.Y., and Mooney, D.J. (2001). Hydrogels for tissue engineering. Chem. Rev. *101*, 1869–1880.

Lee, Y., Song, W.J., and Sun, J.-Y. (2020). Hydrogel soft robotics. Mater. Today Phys. *15*, 100258.

Li, J., and Mooney, D.J. (2016). Designing hydrogels for controlled drug delivery. Nat. Rev. Mater. *1*, 1–17.

Lin, C., Lv, J., Li, Y., Zhang, F., Li, J., Liu, Y., Liu, L., and Leng, J. (2019). 4D-printed biodegradable and remotely controllable shape memory occlusion devices. Adv. Funct. Mater. *29*, 1906569.

Lipson, H., and Kurman, M. (2013). Fabricated: The New World of 3D Printing (John Wiley & Sons).

Liu, J., Qu, S., Suo, Z., and Yang, W. (2021). Functional hydrogel coatings. Natl. Sci. Rev. *8*, nwaa254.

Liu, Q., Nian, G., Yang, C., Qu, S., and Suo, Z. (2018a). Bonding dissimilar polymer networks in

various manufacturing processes. Nat. Commun. *9*, 846.

Liu, X., Yuk, H., Lin, S., Parada, G.A., Tang, T.-C., Tham, E., Fuente-Nunez, C.de la, Lu, T.K., and Zhao, X. (2018b). 3D printing of living responsive materials and devices. Adv. Mater. *30*, 1704821.

Liu, X., Liu, J., Lin, S., and Zhao, X. (2020). Hydrogel machines. Mater. Today *36*, 102–124.

Ma, X., Liu, J., Zhu, W., Tang, M., Lawrence, N., Yu, C., Gou, M., and Chen, S. (2018). 3D bioprinting of functional tissue models for personalized drug screening and in vitro disease modeling. Adv. Drug Deliv. Rev. *132*, 235–251.

Muth, J.T., Vogt, D.M., Truby, R.L., Mengüç, Y., Kolesky, D.B., Wood, R.J., and Lewis, J.A. (2014). Embedded 3D printing of strain sensors within highly stretchable elastomers. Adv. Mater. *26*, 6307–6312.

Ouyang, L., Highley, C.B., Sun, W., and Burdick, J.A. (2017). A generalizable strategy for the 3D bioprinting of hydrogels from nonviscous photo-crosslinkable inks. Adv. Mater. *29*, 1604983.

Skylar-Scott, M.A., Mueller, J., Visser, C.W., and Lewis, J.A. (2019). Voxelated soft matter via multimaterial multinozzle 3D printing. Nature *575*, 330–335.

Smay, J.E., Cesarano, J., Tuttle, B.A., and Lewis, J.A. (2002). Piezoelectric properties of 3-X periodic $Pb(Zr_xTi_{1-x})O_3$–polymer composites. J. Appl. Phys. *92*, 6119–6127.

Su, R., Wen, J., Su, Q., Wiederoder, M.S., Koester, S.J., Uzarski, J.R., and McAlpine, M.C. (2020). 3D printed self-supporting elastomeric structures for multifunctional microfluidics. Sci. Adv. *6*, eabc9846.

Sun, J.-Y., Zhao, X., Illeperuma, W.R.K., Chaudhuri, O., Oh, K.H., Mooney, D.J., Vlassak, J.J., and Suo, Z. (2012). Highly stretchable and tough hydrogels. Nature *489*, 133–136.

Thiele, J., Ma, Y., Bruekers, S.M.C., Ma, S., and Huck, W.T.S. (2014). 25th anniversary article: designer hydrogels for cell cultures: a materials selection guide. Adv. Mater. *26*, 125–148.

Tian, K., Bae, J., Bakarich, S.E., Yang, C., Gately, R.D., Spinks, G.M., in het Panhuis, M., Suo, Z., and Vlassak, J.J. (2017). 3D printing of transparent and conductive heterogeneous hydrogel–elastomer systems. Adv. Mater. *29*, 1604827.

Truby, R.L., and Lewis, J.A. (2016). Printing soft matter in three dimensions. Nature *540*, 371–378.

Wallin, T.J., Pikul, J., and Shepherd, R.F. (2018). 3D printing of soft robotic systems. Nat. Rev. Mater. *3*, 84–100.

Wang, J., Lu, T., Yang, M., Sun, D., Xia, Y., and Wang, T. (2019). Hydrogel 3D printing with the capacitor edge effect. Sci. Adv. *5*, eaau8769.

Wehner, M., Truby, R.L., Fitzgerald, D.J., Mosadegh, B., Whitesides, G.M., Lewis, J.A., and Wood, R.J. (2016). An integrated design and fabrication strategy for entirely soft, autonomous robots. Nature *536*, 451–455.

Wichterle, O., and Lím, D. (1960). Hydrophilic gels for biological use. Nature *185*, 117–118.

Yang, C., Cheng, S., Yao, X., Nian, G., Liu, Q., and Suo, Z. (2020). Ionotronic luminescent fibers, fabrics, and other configurations. Adv. Mater. *32*, 2005545.

Yang, C., and Suo, Z. (2018). Hydrogel ionotronics. Nat. Rev. Mater. *3*, 125–142.

Yang, C.H., Chen, B., Lu, J.J., Yang, J.H., Zhou, J., Chen, Y.M., and Suo, Z. (2015). Ionic cable. Extreme Mech. Lett. *3*, 59–65.

Yang, C.H., Chen, B., Zhou, J., Chen, Y.M., and Suo, Z. (2016). Electroluminescence of giant stretchability. Adv. Mater. *28*, 4480–4484.

Yang, C.H., Wang, M.X., Haider, H., Yang, J.H., Sun, J.-Y., Chen, Y.M., Zhou, J., and Suo, Z. (2013). Strengthening alginate/polyacrylamide hydrogels using various multivalent cations. ACS Appl. Mater. Interfaces *5*, 10418–10422.

Yang, H., Li, C., Yang, M., Pan, Y., Yin, Q., Tang, J., Qi, H.J., and Suo, Z. (2019). Printing hydrogels and elastomers in arbitrary sequence with strong adhesion. Adv. Funct. Mater. *29*, 1901721.

Zhang, F., Wang, L., Zheng, Z., Liu, Y., and Leng, J. (2019a). Magnetic programming of 4D printed shape memory composite structures. Compos. A Appl. Sci. Manuf. *125*, 105571.

Zhang, Y., Shi, G., Qin, J., Lowe, S.E., Zhang, S., Zhao, H., and Zhong, Y.L. (2019b). Recent progress of direct ink writing of electronic components for advanced wearable devices. ACS Appl. Electron. Mater. *1*, 1718–1734.

Zhang, P., Li, Q., Xiao, Y., and Yang, C. (2021a). Biomimetic hydrophilic Islands for integrating elastomers and hydrogels of regulable curved profiles. ACS Appl. Electron. Mater. *3*, 668–675.

Zhang, W., Wang, H., Wang, H., Chan, J.Y.E., Liu, H., Zhang, B., Zhang, Y.-F., Agarwal, K., Yang, X., Ranganath, A.S., et al. (2021b). Structural multi-colour invisible inks with submicron 4D printing of shape memory polymers. Nat. Commun. *12*, 112.

Zhou, L.-Y., Fu, J., and He, Y. (2020). A review of 3D printing technologies for soft polymer materials. Adv. Funct. Mater. *30*, 2000187.

**iScience, Volume *24***

## Supplemental information

# Direct-ink-write printing of hydrogels using dilute inks

**Xiaotian Li, Ping Zhang, Qi Li, Huiru Wang, and Canhui Yang**

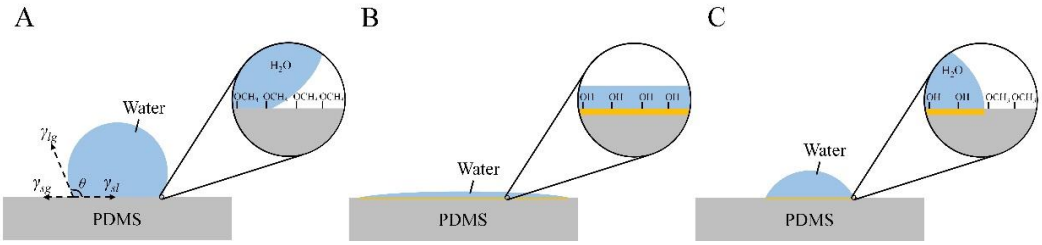


**Figure S1.** Wetting behaviors of water on PDMS elastomers of different surface energy mappings, related to Figure 2. (A) A water droplet beads up on hydrophobic surface of PDMS, which is rich in methyl groups. An obtuse contact angle forms at the triple point. Neglect the deformation of PDMS elastomer, the contact angle is determined by Young's equation, $\gamma_{sg} - \gamma_{sl} - \gamma_{lg}\cos\theta = 0$, where $\gamma_{sg}$ is the solid–gas interfacial energy, $\gamma_{sl}$ the solid–liquid interfacial energy, $\gamma_{lg}$ the liquid–gas interfacial energy, and $\theta$ the contact angle. (B) A water droplet wets well on hydrophilic surface of PDMS, which is rich in hydroxyl groups. (C) A water droplet wets and resides within the hydrophilic region on the surface of PDMS.

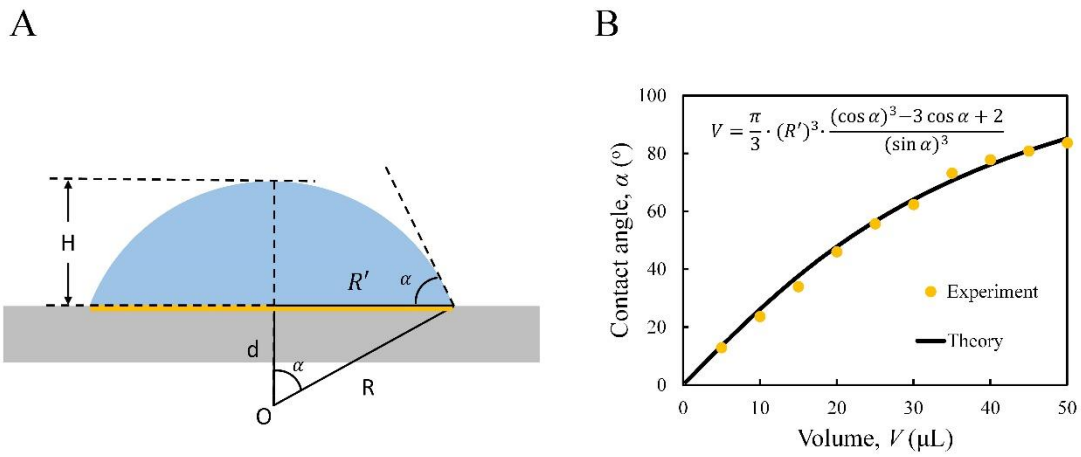


**Figure S2.** Control and maintenance of the shape of dilute ink on the partially plasma etched PDMS after deposition by adjusting the volume of ink, related to Figure 2. (A) Schematic showing the profile of the ink after deposition. A spherical cap is assumed. (B) Contact angle as a function of volume for experiment and theory. The experimental data are taken from Ref. 32. Theorical predication is in good agreement with experimental data.

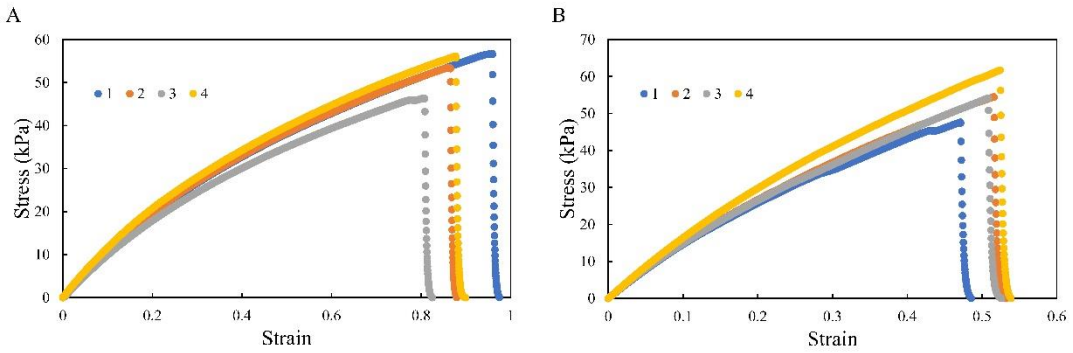


**Figure S3.** S-S curves of hydrogels cured by (A) LAP in the open air and (B) *α*-ketoglutarate in molds, related to Figure 2.


**Figure S4.** A printed “SUSTECH” PAAm hydrogel pattern on PDMS elastomer, related to Figure 2. The PAAm hydrogel is colored with orange dye.

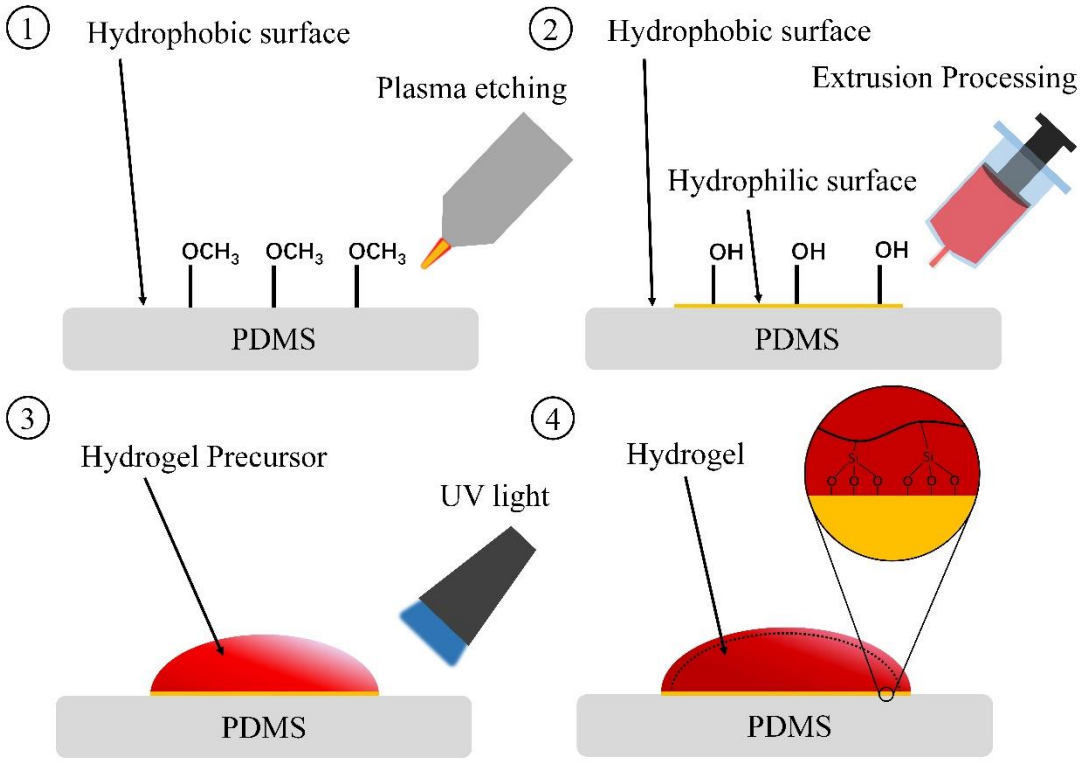


**Figure S5.** Schematic of printing and curing of PAAm hydrogel on PDMS elastomer, related to Figure 2. First, the surface of PDMS is partially plasma-etched and the etched regions have exposed -OH groups. Second, PAAm hydrogel precursor is extruded out of deposition nozzle. The hydrogel precursor spontaneously spreads over and is confined within the plasma-etched regions. Finally, UV light is used to solidify the precursor and the resulting PAAm hydrogel adheres to PDMS elastomer covalently.

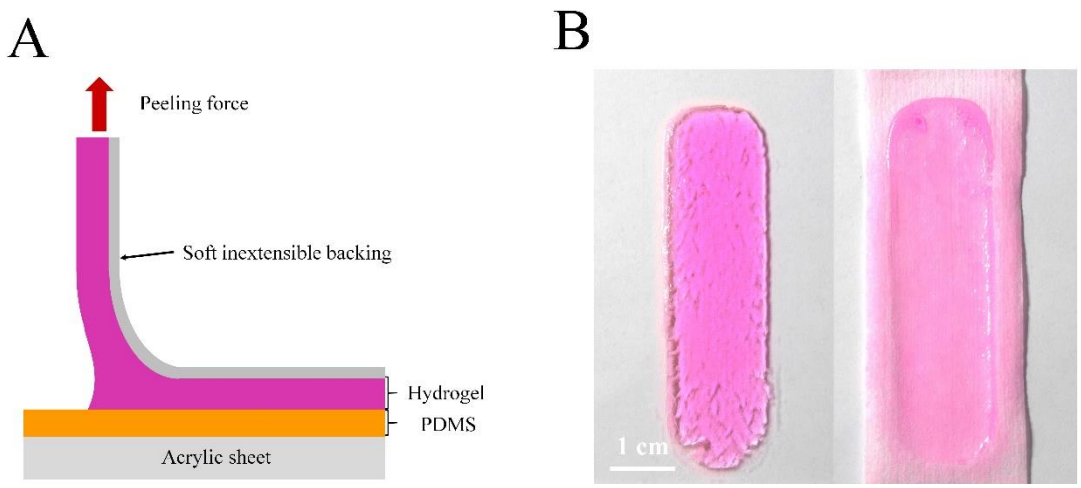


**Figure S6.** 90-degree peel, related to Figure 2. (A) Schematic of 90-degree peel. (B) Digital images of the backing and substrate after peel. Hydrogel residues leave on both sides, indicating cohesive failure.

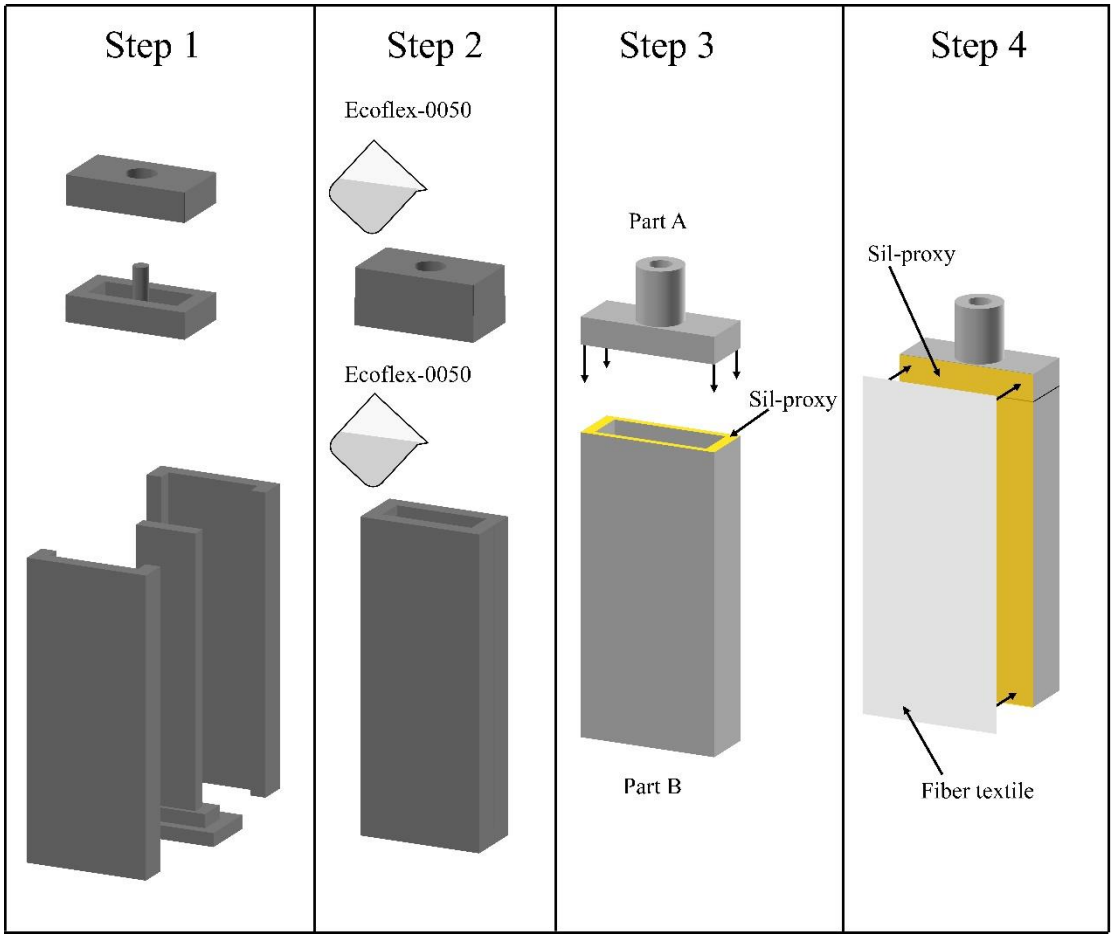


**Figure S7.** Manufacturing of soft muscle, related to Figure 4. Step 1, 3D printing the mold of Part A/B (see step 3). Step 2 fulfill the mold with silicon rubber Ecoflex-0050 and put the sample into 50 ℃ oven half an hour. After curing, demold the sample to get Ecoflex-0050 structure. Cut off the unnecessary parts before further processing. Step 3, paint Sil-poxy glue on the joint surfaces of Part A/B, assemble them together and wait for one hour for curing. Step 4 scissor a fiber cloth with identical dimensions with the soft muscle (yellow-marked surface), paint Sil-proxy glue onto the soft muscle, then align and stick the fiber cloth on it.

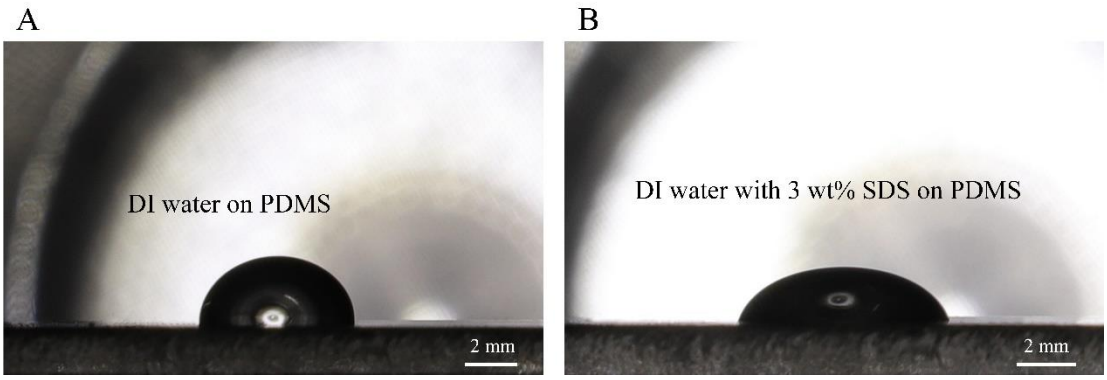


**Figure S8.** Wetting behaviors of water of different surface energies on PDMS elastomer, related to Figure 2. Digital images of (A) 100uL DI water on PDMS, and (B) 100uL DI water with 3 wt% sodium dodecyl sulfate (SDS) on PDMS. Qualitatively, the change of contact angle from obtuse to acute implies the decrease of surface energy. DI water is hydrophilic while DI water with 3 wt% SDS is lipophilic. Also, the relatively large acute contact angle in (B) further implies that the surface energy of DI water with 3 wt% SDS is larger than that of pristine PDMS.

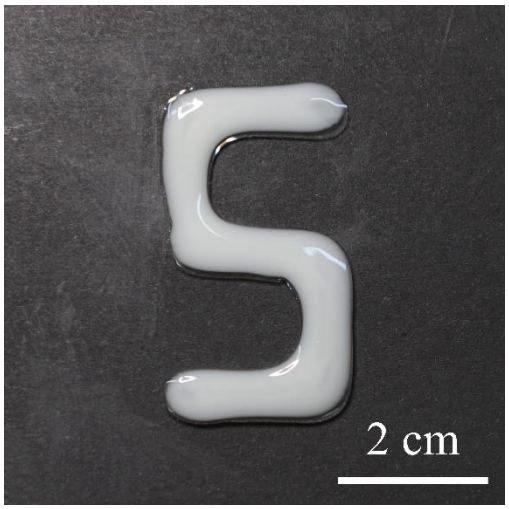


**Figure S9.** Digital image of a printed PAAm ionogel in "S" shape on PDMS elastomer, related to Figure 2. The molar concentration of AAm is 4 mol $L^{-1}$. The ionic liquid is 1-ethyl-3-methylimidazolium ethylsulfate ($[C_2mim][EtSO_4]$). Before curing, the precursor is transparent. After curing, the ionogel is opaque, presumably due to phase separation caused by the incompatibility between PAAm polymer chains and the ionic liquid.

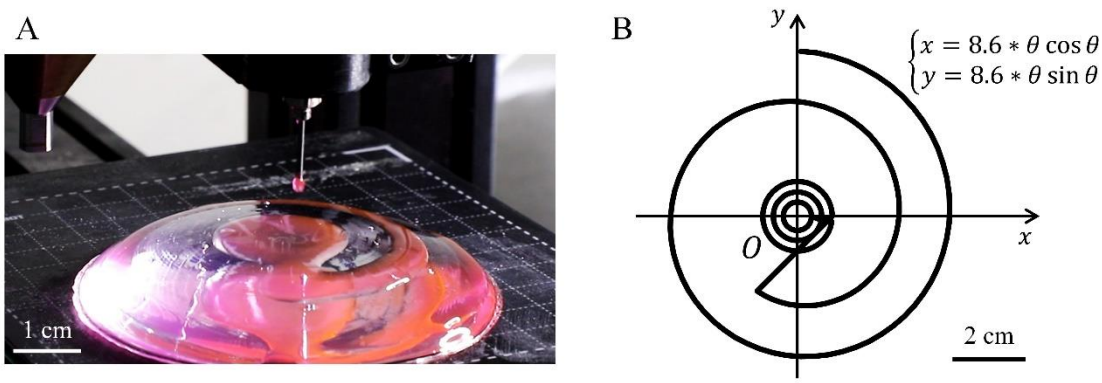


**Figure S10.** Printing on non-planar surface, related to Figure 1. (A) A snapshot of printing the precursor of PAAm hydrogel (colored by red dye) in "Archimedean spiral" pattern on the surface of PDMS substrate. The PDMS substrate is in elliptic cap shape of semi-major axis of 90 mm and semi-minor axis of 30 mm. (B) Schematic and the equation of the "Archimedean spiral" pattern. The central part consists of three circles of radius 17 mm, 12 mm and 7 mm respectively.

## Transparent Methods

**Materials:** We purchase acrylamide (AAm, A108465), N, N'-Methylenebisacrylamide (MBAA, A1922114), lithium phenyl-2,4,6-trimethylbenzoylphosphinate (LAP, L157759), 3-(trimethoxysilyl) propyl methacrylate (TMSPMA, S111153), lithium chloride (E1931129), 1-ethyl-3-methylimidazolium ethylsulfate ([C2mim][EtSO4]), [3-(Methacryloylamino)propyl]trimethylammonium chloride (MAPTAC, C10879476), [2-(Methacryloyloxy)ethyl]dimethyl-(3-sulfopropyl)ammonium Hydroxide (SPE, C10755263), 2-acrylamido-2-methylpropane sulfonic acid (AMPS, CECB120008), acrylic acid (AAc, G2016171), N-isopropylacrylamide

(NIPAM, E2025136), and Rhodamine B (E1914016) from Aladdin, Gelatin-methacryloyl (GelMA) from Suzhou yongxin Co. China, ZnS:Cu particles from Shanghai Keyan Co. China, and polydimethylsiloxane (Sylgard 184) from Dow corning. All chemicals are used as received without further purification.

**Preparation of PDMS elastomer:** precursor of PDMS elastomer is made by mixing the base and crosslinking agents at a weight ratio of 10:1. The precursor is spin-coated on an acrylic sheet at a velocity of 200 rpm for 60 seconds and then stored in an oven at 65 ℃ for 4 hours to cure.

**Preparation of AAm hydrogel precursor:** For 1 mL solution of AAm (8 mol $L^{-1}$ in deionized water), 100 µL 0.5 wt% LAP solution, 24 µL TMSPMA, 32 µL MBAA (0.1 mol $L^{-1}$ in deionized water) are added, followed by vortex mixing for 60 seconds. Lithium chloride (10 mol $L^{-1}$) is added to endow ionic conductivity when needed.

**Preparation of AAc (or AMPS) hydrogel precursor:** For 1 mL solution of AAc (or AMPS) (8 mol $L^{-1}$ in deionized water), 100 µL 0.5 wt% LAP solution, 24 µL TMSPMA, 32 µL MBAA (0.1 mol $L^{-1}$ in deionized water) are added, followed by vortex mixing for 60 seconds.

**Preparation of SPE hydrogel precursor:** For 1 mL solution of SPE (4 mol $L^{-1}$ in deionized water), 100 µL 0.5 wt% LAP solution, 24 µL TMSPMA, 32 µL MBAA (0.1 mol $L^{-1}$ in deionized water) are added, followed by vortex mixing for 60 seconds.

**Preparation of MAPTAC-co-AAm hydrogel precursor:** Because MAPTAC monomer solution by itself does not cure, we copolymerize MAPTAC with AAm to form a copolymer hydrogel. For 1 mL solution of MAPTAC (2 mol $L^{-1}$ in deionized water) and AAm (6 mol $L^{-1}$ in deionized water), 100 µL 0.5 wt% LAP

solution, 24 μL TMSPMA, 32 μL MBAA (0.1 mol $L^{-1}$ in deionized water) are added, followed by vortex mixing for 60 seconds.

**Preparation of NIPAM hydrogel precursor:** For 1 mL solution of NIPAM (4 mol $L^{-1}$ in deionized water), 100 μL 0.5 wt% LAP solution, 24 μL TMSPMA, 32 μL MBAA (0.1 mol $L^{-1}$ in deionized water) are added, followed by vortex mixing for 60 seconds.

**Preparation of GelMA precursor:** For 1 mL solution of GelMA (20 wt% in deionized water), 100 μL 0.5 wt% LAP solution, 24 μL TMSPMA, 32 μL MBAA (0.1 mol $L^{-1}$ in deionized water) are added, followed by vortex mixing for 60 seconds.

**Preparation of hydrogel precursor cured by *α*-ketoglutarate**: For 1 mL solution of AAm (8 mol $L^{-1}$ in deionized water), 80 μL 0.1 mol $L^{-1}$ *α*-ketoglutarate solution, 24 μL TMSPMA, 32 μL MBAA (0.1 mol $L^{-1}$ in deionized water) are added, followed by vortex mixing for 60 seconds.

**90-degree peel test:** Before test, silane modified hydrogels are cured onto the partially plasma-etched PDMS surfaces with the normalized size of 90 × 20 × 1.11 (length × width × thickness) $mm^3$. Then the samples are sealed in a polyethylene bag and kept in oven at 65 ℃ for 1 h. After that, a soft backing layer (non-woven fabric, ~25 μm thick) is glued onto the top side of each hydrogel to prevent elongation of hydrogel along the peeling direction. The resultant samples are all measured using the standard 90-peeling test at room temperature with a mechanical testing machine (100 N load cell; INSTRON 5966) and a constant peeling speed of 20 mm $min^{-1}$.

**Tensile test**: Before test, hydrogels are cured inside molds made of PMMA with the sizes of 60 × 20 × 2 (length × width × thickness) $mm^3$. After curing, the

samples are taken out and subjected to tensile test by using a mechanical testing machine (100 N load cell; INSTRON 5966) at room temperature and constant elongation velocity of 20 mm $min^{-1}$.

**Printing "SUSTECH" pattern:** A layer of PDMS elastomer is spin coated on an acrylic sheet, cured in oven at 65 ℃ for 4 hours, and then placed on the printing platform. A "SUSTECH" pattern is encoded into a G-code file and imported via the controlling system to the printing machine to execute the patterning twice: one for the plasma torch and the other for the deposition nozzle. After printing, an ultra-violet lamp with a wavelength of 405 nm is irradiated for solidification. Finally, the hydrogel is dip-coated with an additional layer of PDMS elastomer and the sample is separated from the acrylic plate.

**Fabrication of ionotronic luminescent device:** ZnS:Cu phosphor particles are added into the precursor of PDMS at weight ratio of 1:10 and mixed thoroughly to obtain a homogeneous solution. The solution is spin-coated on acrylic plate at a velocity of 200 rpm for 60 seconds. After curing in 65 ℃ oven for 4 hours, the electroluminescent layer is obtained, taken out and placed on the printing platform. Hydrophilic regions in a "SUSTECH" pattern are made on the surface of electroluminescent layer and PAAm hydrogel electrodes in the same pattern are printed as previously described. After that, the sample is sealed in a plastic bag and stored at 65 ℃ for 1 hours, during which the silanes on PAAm polymers condense with the hydroxyl groups on PDMS to engender strong adhesion. Then a copper wire is put in contact with the hydrogel electrode and sealed by a layer of PDMS elastomer to prevent accidental short circuit. Finally, another layer of PAAm hydrogel is made on the other side of the

electroluminescent layer. When voltage is applied on the two layers of hydrogel, the phosphor particles emit light to display the “SUSTECH” pattern.

**Printing hydrogel sensor for soft muscle:** The fabricated soft muscle is installed placed on the printing platform. A "U" shaped pattern is encoded into the G-code file and imported into the printing machine through the control system to operate twice: one for the plasma torch to make regions of higher surface energy and the other for the deposition nozzle to eject hydrogel precursor. After printing, an ultra-violet lamp with a wavelength of 405 nm is irradiated for solidification.

**Analysis for the control and maintenance of the shape of dilute ink on the partially plasma etched PDMS after deposition by adjusting the volume of ink:** Assume that the plasma etched region (yellow-marked in Figure S2A) is circle. A small droplet of ink is deposited onto the region. Surface tension prevails and the gravitational effect is negligible, such that the droplet takes a spherical cap profile. Let *V* be the volume of the deposited ink, *H* the height of spherical cap, *α* the contact angle, *R* the radius of spherical cap, *R*’ the radius of plasma-etched region, and *d* the distance from the center of the sphere to the contact surface.

The volume of spherical cap is:

$$V = \frac{\pi}{3} \cdot (3R - H)H^2$$

Geometrically,

$$R = \frac{R'}{sin\,\alpha}; d = \frac{R'}{tan\,\alpha}$$

*H* is obtained as:

$$H = R - d = \frac{R'}{sin\,\alpha} - \frac{R'}{tan\,\alpha}$$

Substitute *H* and *R* into the first equation and rearrange, we obtain:

$$V = \frac{\pi}{3} \cdot (R')^3 \cdot \frac{(cos\,\alpha)^3 - 3\,cos\,\alpha + 2}{(sin\,\alpha)^3}$$

When the dilute ink is deionized water and *R*' = 3 mm, we plot contact angle as a function of volume (solid line in Figure S2B), which satisfactorily agrees with experimental measurements (data points in Figure 3B, taken from Reference 32). Note that when the volume becomes too large, the effect of gravity cannot be neglected, and the droplet will be flattened. Further increase in volume will cause the droplet to spread out of the plasma etched region. Thereafter, the wetting behavior of droplet will recover to that on pristine PDMS elastomer.

The above discussion is valid provided that the surface tension of the ink is larger than that of pristine substrate, otherwise it will be energetically favorable for the ink to spread over the pristine substrate. In addition, when the surface tension of the ink is larger than that of pristine substrate, the ultimate shape of the ink is independent of surface energy. Of course, when viscosity increases, the ink may not spread over the plasma-etched region.

**Note S1: G-code for "S" pattern.** ; Note: sentences starting with ";" are annotations.

M82 ; Prepare the request

G28 ; Auto home all axes

G1 F3000 Z15.0 ; Set the feed rate of subsequent moves to 3000 mm $min^{-1}$, and move to coordinate 15.0 on Z axis

```
G92                         E-3          ; Set the position of
extruder to -3
M107                                     ; Turn off cooling fan
G1    F3600 X108  Y75                    ; Set the feed rate of
```

subsequent moves to 3600 mm $min^{-1}$ and move to coordinate 108 on X axis and 75 on Y axis.

```
G1    F3600 X108  Y75   Z0.12
G1    F550  X96   Y75
G1          X96   Y63
G1          X108  Y63
G1          X108  Y51
G1          X94   Y51
G1    F3600             Z20
G1    F3600 X67   Y112  Z0.12 E0
G1    F550  X65   Y112
G1          X53   Y112       E2.5
G1          X53   Y100       E5
G1          X65   Y100       E7.5
G1          X65   Y88        E10
G1          X53   Y88        E12.5
G1    F3600             Z20
G28
M84
M82
```